Journal of Materials and Electronic Devices 1(2016) 16-21

Grain-Size Effects on the Structural and Electrical Properties of Iron–Based Nano-Crystalline Glass-Ceramic

Omar A. Al-Hartomy[a,b], Ahmed A. Al-Ghamdi[b], M.M. El-Desoky[c], Farid El-Tantawy[d,e], W. A. Farooq[f]

[a]*Department of physics, Faculty of Science, Tabuk University, Tabuk 71491, Saudia Arabia*
[b]*Department of Physics, Faculty of Science, ,AL Faisaliah Campus, King Abdulaziz University, Jeddah 21589, Saudi Arabia*
[c]*Department of physics, Faculty of Science, Suez University, Suez, Egypt*
[d]*Department of Physics, Faculty of Science, Suez Canal University, Ismailia, Egypt*
[e]*Center of Nanotechnology, King Abdulaziz University, Jeddah, Saudi Arabia*
[f]*Department of Physics and Astronomy, College of Science, King Saud University, Riyadh, Saudi Arabia*

$35Fe_2O_3$-$20Bi_2O_3$-$45P_2O_5$ glass was produced by conventional melt-quenching method. The structural of the present glass and its heat treated samples were studied by using scanning electron micrographs (SEM), X- ray diffraction (XRD) and differential thermal analysis (DTA) techniques. The nano-crystalline glass ceramic obtained by heat treated at T_{Cl} for 2h exhibits giant improvement of electrical conductivity up to about five orders of magnitude. The conductivity enhancement was attributed to interfacial regions surrounding crystalline grains. However, the glass heat treated at T_{cl} for 4,8 and 24 h the microstructure changes considerably. When grains are large and amorphous phase disappears, then these interfacial regions also vanish and conductivity of the material considerably decreases. The enhancement of electrical conductivity results during nanocrystallization were discussed in terms of a model proposed in this paper and based on a “core-shell” concept.

Keywords: nanostructures, annealing, differential thermal analysis
Submission date:11 December 2015
Acceptance date:12 May 2016

Corresponding authors: aghamdi90@hotmail.com (Ahmed. A. Al-Ghamdi)

1. Introduction

Nano-technology and nanomaterials are considered to be the very important technologies of the 21st century. Nano-crystalline glass ceramics are important because of their new physical properties which are not obtainable in other nanomaterials [1-4]. The nano-crystalline glass ceramics can be formed with a large diversity of crystal types and sizes (nano, micro etc.). Crystal and grain sizes are the most significant structure parameters in electronic nano-crystalline glassy phases [3-8]. These electronic nano-crystalline glassy phases are very high electrical conductivity and high thermal stability [1,2]. This is attributed to the presence of transition metal oxides (TMO) on nano-crystalline forms [1,3]. The high electrical conductivity of nano-crystalline glass ceramics is very responsive to changes in grain size. Recently, the grain-size effects on the electrical properties have been extensively investigated and attention was mainly focused on the TMO such as: V_2O_5, Fe_2O_3 … etc.[1,5].

Lately, there are relatively few reports on iron containing semiconductor glasses [5,9]. Among Fe ion containing oxide glasses and nano-crystalline glass ceramics are types that exhibit magnetism; ferromagnetism is observed in glasses of Fe_2O_3- PbO_2 –Bi_2O_3 [5] and Li_2O_3 – Bi_2O_3 – Fe_2O_3 system [9]. Thus, iron ion containing glasses are expected to show ferromagnetism as well as semiconducting behavior, if any glasses or nano-crystalline glass ceramics containing iron ion have a high electrical conductivity at room temperature and high thermal stability. Electrical conductivity of glasses containing transition metal oxide can be improved by nanocrystallization. The conductivity enhancement caused by the existence of nanocrystalline grains is generally ascribed to creation of extremely defective regions around the grains. One the other hand, it is widely known that many important characteristics of nanomaterials originate from the defective nature of the interfaces between crystalline and amorphous phases [5-7]. The interface regions of higher than average conductivity form a kind of "easy conduction paths" for electrons [8].

The purpose of the present work was to study the grain-size effects on structural and the electrical conductivity improvement of the $35Fe_2O_3$-$20Bi_2O_3$-$45P_2O_5$ nano-crystalline glass ceramic. The crystal structural and electrical conductivity improvement of the present were investigated as a function of the grain-size using DTA, XRD, SEM and dc conductivity measurements, respectively.

2. Experimental details

Glass with composition $35Fe_2O_3$-$20Bi_2O_3$-$45P_2O_5$ was fabricated via the melt quenching technique. Well mixed powders containing appropriate amounts of reagent grade P_2O_5 (99.999%), Bi_2O_3(99.999%) and Fe_2O_3 (99.99%) were melted at 1100^{o}C for 0.5 h in an electric muffle furnace. Pair of steel blocks was used to quench the melts into 2 mm thick plates. The nano-crystalline glass ceramic was prepared by thermal nanocrystalization of the above mentioned glass by heating in air at crystallization temperature T_{cI} for different times 0, 2, 4, 8 and 24h. X-ray powder diffraction (XRD) studies were performed at room temperature using a Shimatzou XRD-6000 on the as-quenched and heat-treated samples at different times to confirm their amorphous and crystalline states, respectively. The X-rays from a copper tube were monochromated with a graphite crystal to give monochromatic Kα1 radiation. A gas-filled proportional counter collects data over the range 10° to 50° in steps of 0.02°.The glassy state of the as-quenched sample was established by using Shimatzou DTA 50 instrument with a heating rate 15 ^{o}C min^{-1} in the temperature range from room temperature to 800 ^{o}C under air- atmosphere. Scanning Electron Micrograph (SEM) studies were performed at room temperature using a JEOLl-5800LV on the as-quenched and heat-treated on the interior of samples. The dc electrical conductivity (σ) of the present glass and its nano-crystalline glass ceramic were performed by using two point-probe method. A multimeter type Keithely 760 was used to collect data. Silver paste electrodes deposited on both flanes of the polished samples.

3. Results and discussion

3.1. Differential thermal analysis

The as-quenched glass sample was subjected of differential thermal analysis (DTA) to measure glass transition (T_g), crystallization temperatures (T_{CI} and T_{CI}) and melting temperature (T_m)**.** Fig. (1) exhibits an endothermic dip due to T_g, two exothermic peaks corresponding to crystallization ($T_{CI,}T_{CII}$) and endothermic dip due to T_m .The DTA for as–quenched glass has an endothermic dip at T_g =373 ^{o}C , an exothermic peak at T_{CI} =424 ^{o}C followed by another exothermic peak at T_{CII} =637 ^{o}C and an endothermic dip at T_m=780 ^{o}C . However, the thermal stability of a glass depends on the temperature difference $\Delta T = T_{CI}$. -T_g of the sample [10]. A significant difference between the glass transition, T_g (373 ^{o}C) and the crystallization T_{CI} (424 ^{o}C) temperatures accounts for good thermal stability of the $35Fe_2O_3$-$20Bi_2O_3$-$45P_2O_5$ glass. The difference between T_g and T_{CI} is 51 ^{o}C for the present glass. However, the thermal stability of the glass could also be expected by the factor T_g/T_m. For very stable glass the perfect value of T_g/T_m is 0.67 [6]. The T_g/T_m value in present glass falls in the range 0.613 being near to that of the perfect value [10].

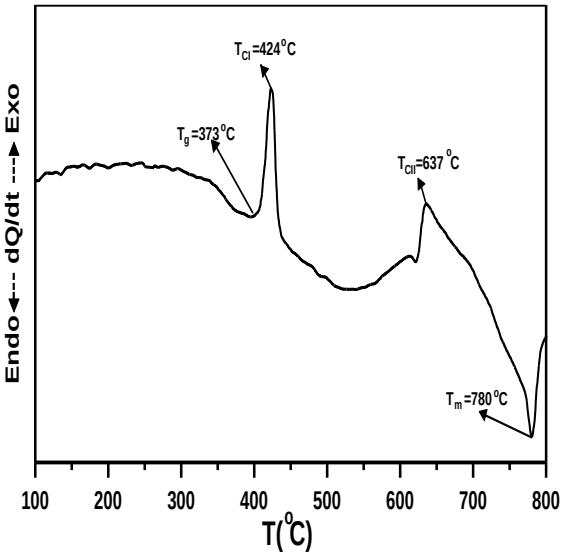

Fig.1: Differential thermal analysis (DTA) of $35Fe_2O_3$-$20Bi_2O_3$-$45P_2O_5$ glass.

3.2. Scanning Electron Microscopy Studies

Scanning Electron Micrograph (SEM) of $35Fe_2O_3$-$20Bi_2O_3$-$45P_2O_5$ glass sample at different heat treated times 0, 2, 4, 8 and 24h are shown in Fig. (2a-e), respectively at T_{CI}=424^{o}C. The micrograph of as-quenched glass sample (Fig.2a) exhibits a surface without the presence

of microstructure. This approves the amorphous state of as-quenched glass [6].

Fig.2b shows SEM for the sample heat treated at crystallization temperature (T_{CI}) for 2 h, indicates thepresence of many crystallites of different grain sizes distributed in the glassy matrix. The average grain size of these is generally about 95nm. Further nanocrystallites one can see some remnant glassy phase. However, Fig.2c and d shows SEM of heat treated samples at T_{CI} for 4 h and 8h, appearances the presence of many crystallites of grain sizes 0.4-0.8 μm and 0.6-0.2μm, respectively distributed in the glassy matrix. The grains noticeable in Fig.2c and d do not have regular shape, which should be expected if they were similar crystallites. At present one can see that smaller grains have tendency to form agglomerates also there is an insignificant portion of the remaining amorphous phase [6].

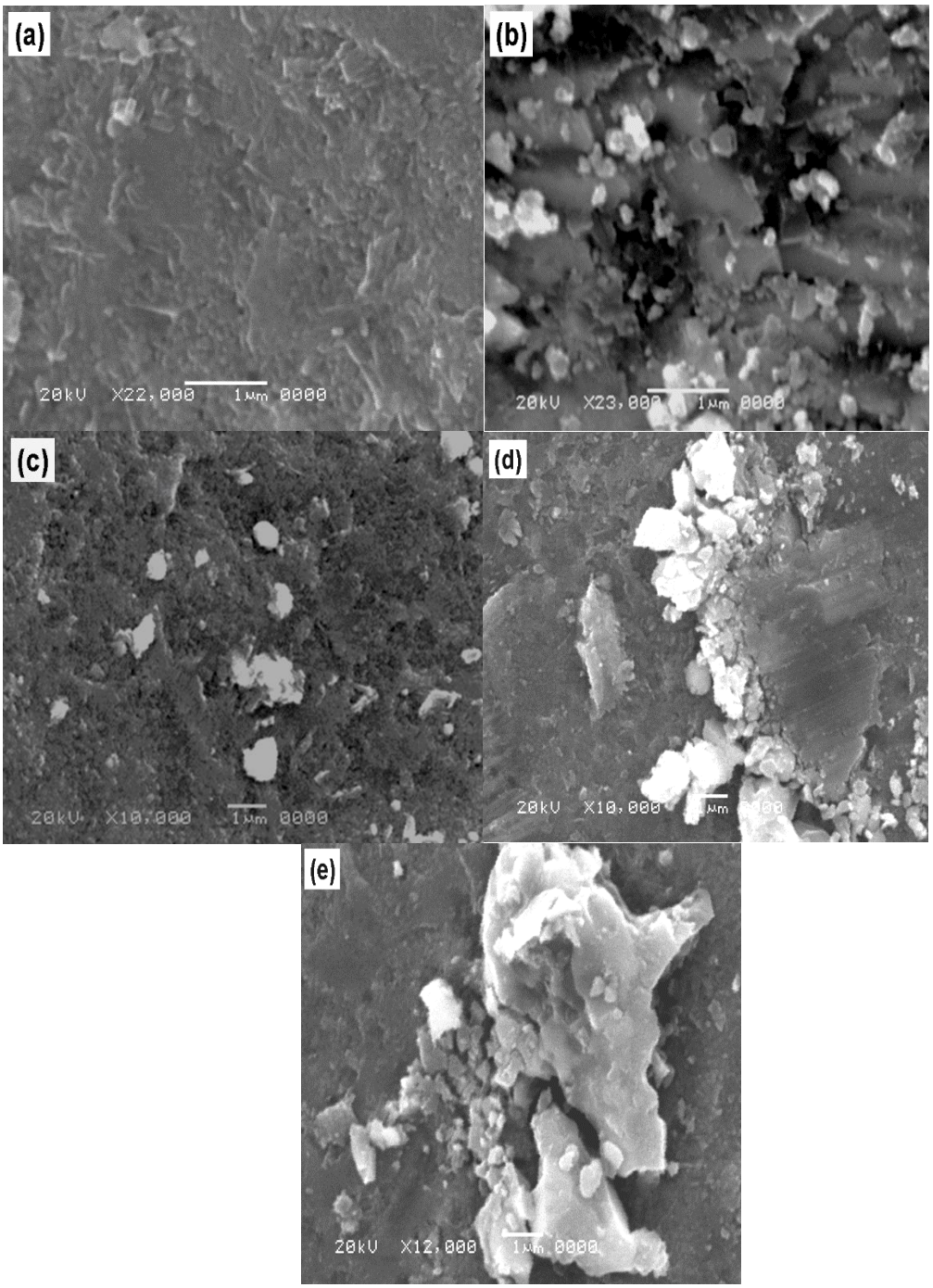

Fig.2: Scanning electron micrographs (SEM) for (a) as- received glass,(b) heat treated (2h), (c) heat treated (4h), (d) heat treated (8)and (e) heat treated (24h) .

The sample heat treated at T_{CI} for 24h a massive crystallization and the microstructure changes significantly (Fig.2e) [3,6]. Also, in this case the grains implanted in the glass [6]. The sample heat treated at T_{CI} for 24 h a massive crystallization and the microstructure changes significantly (Fig.2e) [3,6]. Also, in this case the grains implanted in the glass matrix are well developed [1]. The average dimensions of the grain sizes are usually about 2.3µm.

3.3. X- Ray Diffraction

The X- ray diffraction patterns (XRD) of the present sample at different heat treatment times 0,2,4,8 and 24h, respectively are shown in Fig. (3a-e). In the case of as-prepared glass (Fig. 3a), there is only a wide halo detected with no indication of diffraction peaks. This approves the amorphous state of initial glass. A pattern shown in Fig.3b was studied for a sample heat treated at T_{CI} for 2h [1-5]. It contains a number of diffraction peaks equivalent to a crystalline phase superimposed on a wide halo representing that there is still significant quantity of glassy phase. Average grain size of crystallites was approached from the widths of diffraction peaks, using the Scherrer Eq., is about 90 nm [1-5]. The XRD pattern in Fig.3c and d is an obvious indication that heat treated at T_{CI} for 4h and 8h, respectively starts to produce crystallites in the glass matrix. Average grain size of crystallites was calculated from the widths of all diffraction peaks, is about 0.6 and 1.2µm, respectively. The fourth heat treated, at T_{CI} for 24h (Fig.3e) leads to massive crystallization. The diffraction peaks phases for all stages were identified as Fe_2PO_5, Fe_2O_3 and Bi_2O_3.

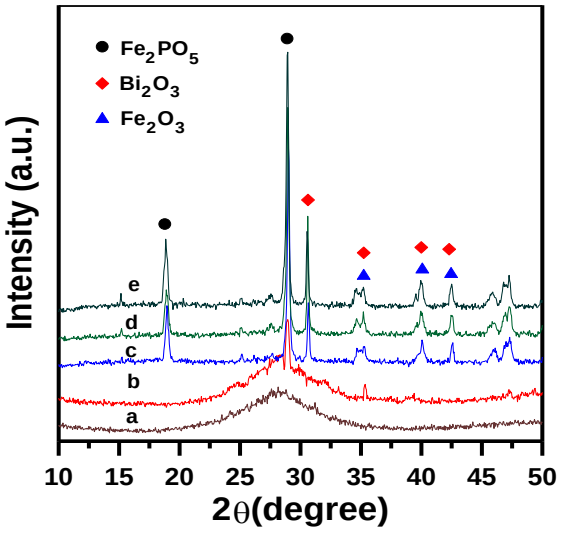

Fig.3: X- ray diffraction (XRD) for (a) as- received glass,(b) heat treated (2h), (c) heat treated (4h), (d) heat treated (8)and (e) heat treated (24h) .

However, there are some new peaks corresponding to the phase which we have not identified yet. The estimate of average grain-size at this stage is close to 2.2µm.

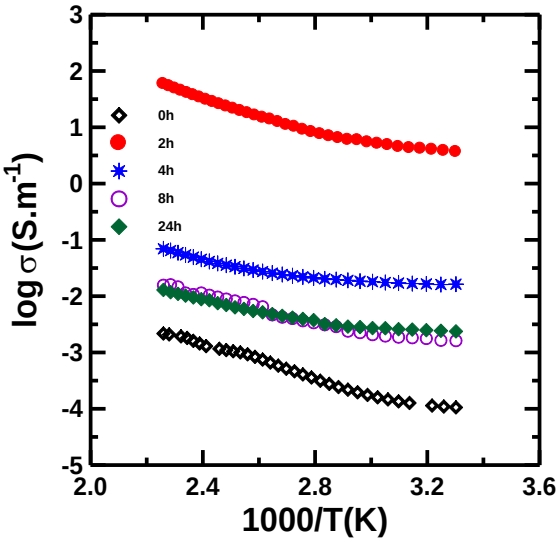

Fig. (4): Temperature dependence of dc conductivity (σ) for 35Fe_2O_3-20Bi_2O_3-45P_2O_5 glass at different heat treatment times.

3.4. dc conductivity

Fig.4 shows the relation between inverse temperature and the dc conductivity, σ, for different heat treatment times (0,2,4,8 and 24h) of 35Fe_2O_3-20Bi_2O_3-45P_2O_5 glass. In particular their electrical conductivity depends on temperature according to Mott formula [11,12].

$$\sigma = \sigma_o \exp(-W/kT) \qquad (1)$$

where W is the activation energy, σ_o is a pre-exponential factor and k is the Boltzmann constant. The electrical conductivity at different stages (Fig.4) exhibits a linear-temperature-dependence up to critical temperature $\theta_D/2$(θ_D Debye temperature) and then the slope changes with deviation from linearity. Similar behavior was found for $BaTiO_3$–V_2O_5–Bi_2O_3 [1] and 20BaO–30V_2O_5–50Bi_2O_3glasses [6]. The slope of each curve which gives the activation energy at high temperature for conduction, however, has two different values, and increases towards higher temperatures [13,14].

Fig.5 shows variations of electrical conductivity at 400K and activation energy as a function of heat treatment times (0,2,4,8 and 24h). From the figure it is clear that, the electrical conductivity passing through a maximum and the activation energy passing through a minimum at time = 2h. This figure suggests a kind of transition in the

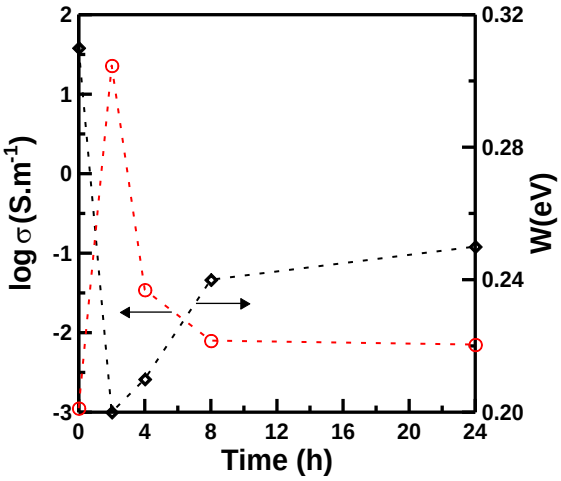

Fig.5: dc conductivity (σ) at 400K and activation energy as a function of heat treatment times. Linear are drowning as guide for eyes.

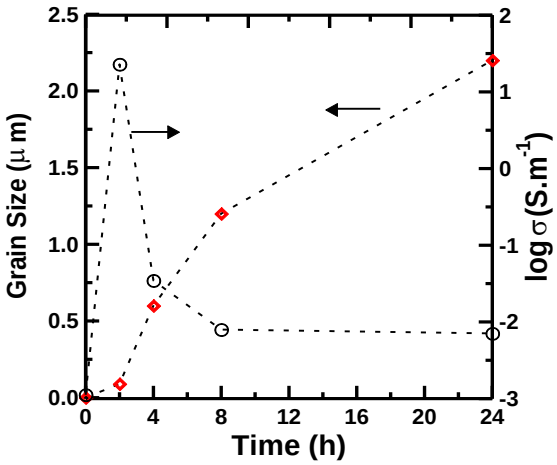

Fig.6: dc conductivity (σ) at 400K and calculate grain size as a function of heat treatment times. Linear are drowning as guide for eyes.

conductive regime. Also, it is show that the electrical conductivity increases while the activation energy decreases with the increase of the heat treatment times or grain size. Such a behavior is a feature of small polaron hopping (SPH) [11,12]. The activation energy ($W_{(2h)}$= 0.2 eV) for the sample heat treated at T_{CI} for 2h are substantially lower than that found for the starting glass ($W_{(0h)}$ = 0.32 eV). The high electrical conductivity and low activation energy after nanocrystallization (2h) is attributed to creation of extensive and dense network of electronic conduction paths which are situated between iron nanocrystals and on their surface [1-7]. In case of the sample heat treated at T_{CI} for 4,8 and 24h shows low conductivity and high activation energy compared to the samples heat treated at 2h [1]. In this case, the conduction paths for electrons "easy conducting paths" are reduced or disappeared and the electrical conductivity considerably decreases [1-3].

The variation of electrical conductivity and calculate grain size as a function of heat treatment times for $35Fe_2O_3$-$20Bi_2O_3$-$45P_2O_5$ glass is shown in Fig.6. It is interesting to note that the heart treatment of the present sample at T_{CI} for 2 h and average grain size (90 nm) exhibits giant improvement of electrical conductivity compared to their as-prepared sample [1-7]. This can be clarified in the following way. The most important for electronic conduction in of the present sample with high concentration of Fe_2O_3 is the spatial distribution of Fe^{2+} and Fe^{3+} ions which are centers of electron hopping [2-5]. In case of as- prepared glass (0h), there is a random distribution of such centers. However, the heat treatment for 2h leads to creation of nanocrystallites (90 nm) of Fe_2O_3 implanted in the glassy matrix. Since the average size of these grains is small than 100 nm, the interface between, crystalline and amorphous phases is very widely separated and strongly effects overall electrical conductivity properties of the nanomaterial as shown in SEM and XRD. Nevertheless, this improvement of electrical conductivity can be attributed to creation of defective, well-conducting regions along the glass-crystallites interfaces [2-6]. In case of heat treatment samples at T_{CI} for 4,8 and 24h and its average grain size 0.8, 1 and 2.2 μm, respectively exhibit a decrease of the electrical conductivity compared to their heat treated at 2h. This is attributed to vanishing of conducting regions or conduction paths for electrons and considerable decrease of electronic conductivity [6].

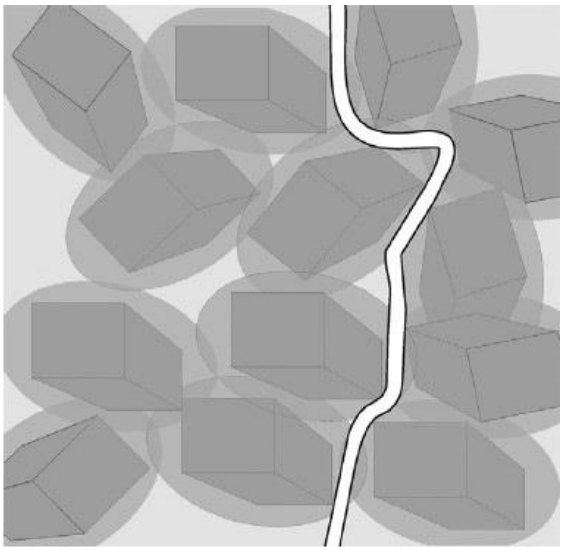

Fig.7: A model of the easy conduction paths in studied nanomaterials using a "core-shell" concept Ref.[3].

On the other hand, to explain the electrical conductivity enhancement during nanocrystallization and decreasing during colossal crystallization it is useful to refer to the well-established core shell model. Pietrzaka et al [3] have discussed this model. Fig.7 shows an illustration of core shell model. For this model a grain consists of an inner completely crystalline "core" and an outer highly disordered, defective and non-stoichiometric "shell"[3]. The same "core-shell" model can clarify the conductivity improvement produced by nanocrystallization. The overlapping and intersecting defective shells around crystalline cores can form a complicated system of paths for facilitated electron transport. The mechanism of electronic transport in iron ions consists in SPH between aliovalent Fe^{2+} and Fe^{3+} sites. In the regions where the local concentration of the Fe^{2+}-Fe^{3+} pairs is high, the conductivity is also high. Such a circumstance takes place inside and around the defective grain-shell areas [1,3]. In case of colossal crystallization, the grains become well-developed crystallites with sharp edges. A negative result of this colossal crystallization is decay of the "easy conduction paths" of the interfacial regions [1,3]. However, the disappearance of the disordered shells due to colossal crystallization causes a considerable conductivity drop.

Conclusions

Grain-size effects on the structural and electrical properties behavior of $35Fe_2O_3$-$20Bi_2O_3$-$45P_2O_5$ glass and its heat treated glass were studied by scanning electron micrographs (SEM), X- ray diffraction (XRD), differential thermal analysis (DTA) and dc conductivity measurements over a wide temperature range. It was possible to find relationship between microstructure and electrical properties of the obtained material and to optimize conditions of its fabrication. The conductivity value increasing first with increasing grain to 90 nm, then decreases with further increasing grain-size large than 100 nm. When crystalline grains are small and their concentration is high, the interface between glass matrix and these grains forms an extensively ramified system of conducting paths for electrons. However, grains are large and amorphous phase disappears, then these interfacial regions also vanish and conductivity of the material considerably decreases. The experimental results were discussed in terms of a model proposed in this paper and based on a "core-shell" concept.

Acknowledgment

The present study is a result of an international collaboration program between University of Tabuk, Tabuk, Saudi Arabia and Suez Canal University, Egypt. The authors gratefully acknowledge the financial support from the University of Tabuk, Project number 0144-1433-S.

References:

[1] M. S. Al-Assiri, M. M. El-Desoky, J. Alloys Comp. 509 (2011) 8937.
[2] M.Y. Hassaan, F.M. Ebrahim, A.G. Mostafa, M.M. El-Desoky, Mater. Chem. Phys. 129 (2011) 380.
[3] T.K. Pietrzak, J.E. Garbarczyk, I. Gorzkowska, M.Wasiucionek,J.L. Nowinski, S. Gierlotka, P. Jozwiak, J. Power Sources 194 (2009) 73.
[4] J.E. Garbarczyk, P. Jozwiak, M. Wasiucionek, J.L. Nowinski, Solid State Ionics 175 (2004) 691.
[5] M. M. El-Desoky, F. A. Ibrahim, A.G. Mostafa, M. Y. Hassaan, Mater. Res. Bull. 45 (2010) 1122.
[6] M.M. El-Desoky, Mater. Chem. Phys. 119 (2010) 389.
[7] M.M. El-Desoky, H.S.S. Zayed, F.A. Ibrahim, H.S. Ragab, Physica B 404 (2009) 4125.
[8] J.E. Garbarczyk, P. Jozwiak, M. Wasiucionek, J.L. Nowinski, J. Power Sources 173 (2007) 743.
[9] S. Nakamura and N. Ichinose, J. Non–Cryst. Solids 95-96, (1987), 849.
[10] E.R. Shaaban, M. Shapaan, Y.B. Saddeek, J. Phys. Condens. Matter 20 (2008), 155108.
[11] N.F. Mott, J. Non-Cryst. Solids 1 (1968) 1.
[12] I.G. Austin, N.F. Mott, Adv. Phys. 18 (1969) 41.
[13] A. Mogus-Milankovic, A. Santic, V. Licina , D.E. Day, J.f Non-Cryst. Solids 351 (2005) 3235.
[14] L. Murawski, J. Mater. Sci. 17(1982) 2155.